This is the manuscript of the article that appeared in final form in **Journal of Industrial and Engineering Chemistry** 95 : 312-324 (2021), which has been published in final form at https://doi.org/10.1016/j.jiec.2021.01.006.

Fine particle flow pattern and region delimitation in fountain confined conical spouted beds

Mikel Tellabide*, Idoia Estiati, Aitor Atxutegi, Haritz Altzibar, Roberto Aguado, Martin Olazar

Department of Chemical Engineering, University of the Basque Country UPV/EHU, P.O. Box 644, E48080 Bilbao (Spain).

Abstract

A novel borescopic technique together with the monitoring of pressure fluctuation signals (Power Spectral Distribution, PSD) has been used to track fine particles and characterize solid flow dynamics in fountain confined conical spouted beds. Radial and axial particle velocity profiles have been obtained for different configurations, and spout-annulus and fountain core-periphery interfaces have been delineated. The downward particle velocities in the annulus peak at intermediate positions in this zone, whereas the upward velocities in the dilute zones (spout and fountain core) peak at the axis or close to this position. Among the different configurations analysed in this work, the system without draft tube shows the greatest vertical particle velocities in almost all the different radial and axial positions. The evolution of the spout size along the bed depends on the configuration used, but all of them differ from those commonly reported in the literature. Thus, the spout expands from the bed bottom to the surface, without any neck at a intermediate bed level. Furthermore, the cross-sectional spout shape has been delineated in the systems with open-sided draft tube, and significant spout expansion is observed due to air percolation from the spout into the annulus through the opened faces. Finally, the average spout diameters of the systems without draft tube and with open-sided draft tubes have been

*Corresponding author
Email address: mikel.tellabide@ehu.eus (Mikel Tellabide)

compared with those predicted by literature correlations. Those proposed by San José et al. and Volpicelli et al. provide the best fit for the configurations without draft tube and with open-sided draft tube, with their relative errors being 9.83% and 8.88%, respectively.

Keywords:
Fine particles, conical spouted bed, fountain confiner, particle image velocimetry, particle velocity, spout shape

---

1. Introduction

The spouted bed regime is well-known as an alternative gas-solid contact method to fixed and fluidized beds, which has been successfully applied to systems where fluidization yielded unsatisfactory performance. Moreover, its main characteristic feature is the cyclic movement of the particles in the reactor, which differs from other gas-solid contact regimes. This technology was originally designed to operate with coarse granular particles (greater than $1\,mm$), as fluidized beds may only operate with very shallow beds with these particles. Thus, wheat drying was the first spouted bed application [1].

Since its discovery, different variants of spouted beds have been developed, as are: conical [2], cylindrical [3], mechanical [4], two-dimensional [5] or slot-rectangular [6]. Conical spouted beds combine the features of cylindrical spouted beds (such as small pressure drop or cyclic movement of particles) with those inherent to their geometry, such as stable operation in a wide range of gas flow rates [7].

The conical spouted bed has been successfully applied in different applications, such as drying of different solids [8], pyrolysis [9], coating [10], combustion [11] or steam gasification [12]. Many of these operations involve the use of fine particles and the study of their hydrodynamic behavior is essential in order to determine the ranges of the operating conditions for a suitable performance. Nevertheless, a crucial parameter delimiting stable operation is the ratio between the gas inlet diameter and particle diameter, D_0/d_p, which must

be smaller than $20 - 30$ to attain spouting regime [13, 14].

Use of different internal devices, such as draft tubes, fountain confiners or both, is essential for stable operation with fine particles. Nevertheless, as reported in a previous paper [15], the evolution of pressure drop with air velocity (characteristic curve) depends on the configuration used (without tube, or with open-sided or nonporous tubes). Therefore, a more detailed knowledge of bed performance is required for an optimum design and use of this equipment in industrial applications. Among the parameters requiring study, particle velocity and spout shape are especially relevant for the development of gas and solid flow models.

Nowadays, a range of particle tracking techniques can be found in the literature and all of them are classified into two groups, as are: intrusive (isokinetic sampling, fiber-optic methods, and so on) and non-intrusive methods (Magnetic Resonance Tomography (MRT), Radioactive Particle Tracking (RPT), Positron Emission Particle Tracking (PEPT), Electrical Capacity Tomography (ECT), Particle Image Velocimetry (PIV), X-ray tomography, and so on). Certain authors defend non-intrusive methods against intrusive ones arguing that the probe causes local disturbances of the gas-solid flow and, furthermore, do not provide full flow field measurements [16, 17, 18, 19, 20, 21, 22, 23].

However, some non-intrusive methods, such as X-ray tomography or MRT, rely on very expensive measurement techniques and they do not allow monitoring single particle trajectories. Techniques such as RPT and PEPT allow direct monitoring of tracer particle trajectories with high spatial resolution for particles moving at velocities of up to $20\,m/s$, but the particle tracer has to be activated by radioactive radiation and can only be used for a given time (around 75 minutes) due to the radioactive decay [24]. Furthermore, the handling of these particles requires special safety procedures, which involve additional complexity in the experimentation. ECT technique is a simple and low cost method, but does not allow 3D particle trajectories and electrostatic interference may influence measurements [25].

Among all the mentioned measurement procedures, optical ones are the most

used, i.e., those based on optical fibers and PIV techniques. Although the former is an intrusive method, and therefore may involve flow disturbance, it has been extensively used for the hydrodynamic characterization of spouted bed systems [26, 27, 28, 29, 30]. This method is suitable to measure particle velocity and bed voidage in dilute zones, but the results obtained in dense flow regions are questionable due to the weak light transmission between the emitting and detecting fiber tips [18, 3, 25].

Furthermore, the PIV method allows mapping out the entire solid flow field and measuring particle velocity [5], spout shape [31] and fountain height [32]; that is, it allows ascertaining the hydrodynamic behavior [33] and the solids mixing index in the bed [34]. However, this method involves the use of two-dimensional or half-column transparent spouted beds, and therefore the internal particle motion cannot be recorded, but only that on the transparent surface. According to certain authors [24], the hydrodynamic behaviour of these beds differs from that of full column ones due to the wall effect.

An interesting aspect involving the modelling of solid flow in spouted beds is the solid cross-flow rate from the annulus into the spout. Accordingly, attempts have been made to measure the spout geometry and different correlations have been proposed for estimating the average spout diameter. Table 1 shows the correlations reported in the literature for calculating the average spout diameter. Most of them have been proposed with data obtained from conical base cylindrical or semicircular columns. In the latter, measurements have usually been made on the flat transparent face assuming the wall effect is negligible. Moreover, the experiments have been conducted with coarse regular particles (glass beads) or granular ones (wheat, millet, seeds, peas, and so on), except the one proposed by Wu et al. [35], who operated with sand at high temperatures. Therefore, different spout shapes have been reported in the literature, as well as several different correlations have been proposed. Overall, these correlations relate the spout diameter with the column diameter, fluid velocity and particle density, and the one by Abdelrazek [36] also includes the stagnant bed height.

Previous papers show the effectiveness of the fountain confiner for attaining a

stable spouting regime with fine particles in conical spouted beds either without draft tube or equipped with draft tubes [37, 38, 15]. Furthermore, new operating regimes with different hydrodynamics patterns from those in conventional spouted beds have been characterized when the fountain confiner is used with fine particles. Thus, the main aim of this study is to delve into the knowledge of the gas-solid hydrodynamics of fine particles in a fountain confined conical spouted bed. Accordingly, particle velocities have been measured by a novel borescopic technique [39], which allowed determining the radial and axial particle velocity profiles, and therefore clearly delineating the interface between the spout and the annulus, as well between the fountain core (particle ascending zone) and periphery (particle descending zone).

2. Experimental

2.1. Equipment and materials

Experimental runs have been carried out in a pilot plant unit described in previous papers [49, 15]. A conical contactor made of polyethylene terephthalate has been used and its main dimensions are shown in Figure 1a.

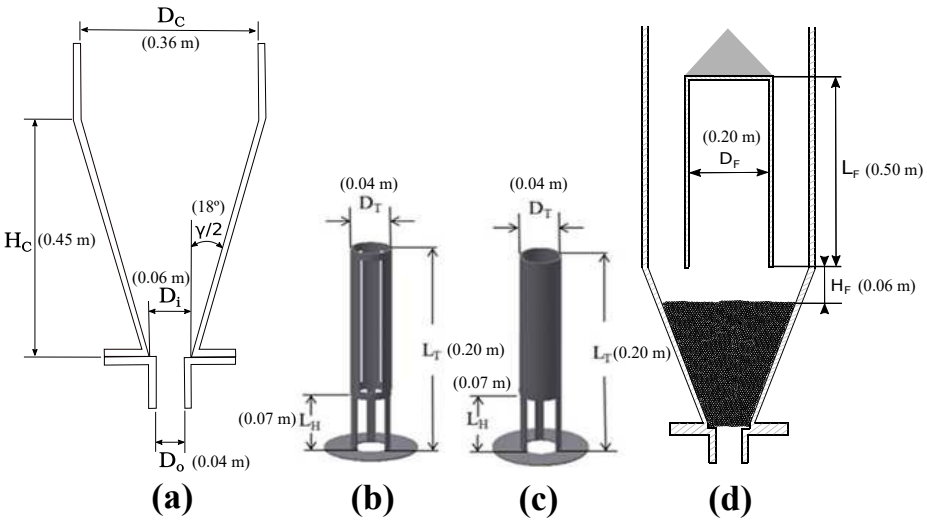

Figure 1: Geometric factors of the (a) conical contactor, (b) open-sided draft tube, (c) non-porous draft tube, and (d) fountain confiner.

Table 1: Literature correlations for calculating the average spout diameter.

Author	**Equation**	
Malek et al. [40]	$\overline{D_s} = \left(4.36 \cdot 10^{-3}\, logD_C + 9.1 \cdot 10^{-3}\right) G^{0.5}$	(1)
Mikhailik [41]	$\overline{D_s} = (1.67\, logD_C + 2.22) \left(\frac{G}{\rho_s}\right)^{0.5}$	(2)
Volpicelli et al. [42]	$\overline{D_s} = (0.13\, logD_C + 0.1793)\, G^{0.5}$	(3)
Lefroy and Davidson [43]	$\overline{D_s} = 1.07\, D_C^{0.75}\, d_p^{0.33}$	(4)
Abdelrazek [36]		
Regular particles	$\overline{D_s} = 0.315\, D_C \left[\frac{u}{(g\, H_0)^{0.5}}\right]^{0.33}$	(5)
Irregular particles	$\overline{D_s} = 0.346\, D_C \left[\frac{u}{(g\, H_0)^{0.5}}\right]^{0.5}$	(6)
McNab [44]	$\overline{D_s} = 2\, D_C^{0.49}\, \frac{D_C^{0.68}}{\rho_b^{0.41}}$	(7)
Bridgwater and Mathur [45]	$\overline{D_s} = 0.384\, G^{0.5}\, \frac{D_C^{0.75}}{\rho_b^{0.25}}$	(8)
Green and Bridgwater [46]	$\overline{D_s} = \left(2 + \frac{D_C}{2}\right) G^{0.49}\, \frac{D_C^{0.68}}{\rho_b^{0.41}}$	(9)
Wu et al. [35]	$\overline{D_s} = 5.61\, G^{0.433}\, \frac{D_C^{0.583}\, \mu^{0.133}}{(\rho_b\, \rho_f\, g)^{0.283}}$	(10)
San José et al. (2001) [47]	$\overline{D_s} = 6.6 \left(\frac{G^{0.4}\, D_C^{0.68}}{\rho_b^{0.41}}\right) \left(\frac{D_0}{D_C}\right) \gamma^{-0.15}$	(11)

Table 1: Continued.

Author	Equation
San José et al. (2005 shallow spouted beds) [30]	$\overline{D_s} = 1.89 \left(\frac{G^{0.49} D_C^{0.68}}{\rho_b^{0.24}} \right) \left(\frac{D_0}{D_C} \right) \gamma^{-0.15}$ (12)
San José et al. (2005 conical spouted beds) [48]	$\overline{D_s} = 0.52\, G^{0.16} D_0^{0.41} \gamma^{-1.19} D_b^{0.8} \left(\frac{u}{u_{ms}} \right)^{0.8}$ (13)

This contactor allows fitting draft tubes at the inlet of the conical section. Thus, particle velocity has been measured in three different configurations, as are: without draft tube, with open-sided draft tube and with nonporous draft tube. The different draft tubes are made of stainless steel and have a cylindrical shape (Figures 1b and 1c). Their main characteristic factor is the aperture ratio (AR), i.e., the fraction of the lateral surface area opened for gas and solid interchange, which is 57% for the open-sided draft tube. Accordingly, the aperture ratio of the configuration without draft tube is 100% and of that with nonporous draft tube 0%.

All the runs have been carried out at the minimum spouting velocity using fine siliceous sand ($\rho_s = 2390\, kg/m^3$) of $0.246\, mm$ average particle diameter. This size has been obtained by sieving in a $CISARP$ 200 N sieve shaker using mesh sizes of 0.2 and $0.3\, mm$, with the result being confirmed in a $Mastersizer$ 2000 laser diffraction particle size analyser. The particle size distribution of the sand can be found in the supplementary material. The particle density has been determined in an *Autopore* 9220 mercury porosimeter from $Micromeritics$.

Given the small size of these particles, a fountain confiner must be used to attain steady and stable spouting. The body of this internal device is a cylindrical tube made of polyethylene terephthalate with the upper end closed to avoid gas and solid leaving the contactor through its top. Additionally, this device is provided with a cone shaped cap on the outer top surface to avoid solid deposition, Figure 1d. The confiner dimensions for stable and efficient spouting

of these solids were determined in previous studies [15, 50], with a distance between the lower end of the device and the bed surface (H_F) of 0.06 m being the optimum to avoid unstable spouting and solid elutriation.

2.2. Experimental procedure

Particle velocity has been measured by a high speed camera fitted to a borescopic system. The camera is an $AOS\ S-PRI$ ($AOS\ Technologies\ AG$) with a maximum recording resolution of 900×700 pixels and a maximum frame rate of up to 16500 frames per second with reduced resolution. Moreover, the borescope optical fiber is connected to a continuous light source and the whole optical system is displaced by a set of sliders, Figure 2a. The use of sliders enables positioning the borescope measuring tip anywhere in the contactor, as shown in Figure 2b. Given that particle velocities differ greatly depending on the zone in the bed, their profiles have been analysed separately, with the axial one corresponding to the axis along the spout and fountain core, and the radial ones to several bed levels, in which solid velocity changes from positive to negative values. It should be noted that all the velocities correspond to the vertical components in both the spout and the annulus. In order to avoid probe perturbations in the bed, this technique has been designed to make the measurement in front of the borescope tip, leaving any perturbation behind the device. The only case in which the measured value may be affected by the rod is the region at the very bottom of the bed, in which the contactor cross sectional area is of the same order as that of the probe. More details about the optical and borescopic systems are provided in a previous paper [39].

The measurements have been carried out in the radial direction at four different heights in each spouted bed region, i.e., spout, annulus and fountain. Therefore, measurements have been carried out at the following heights from the bed bottom to the fountain top: 0.03, 0.11, 0.15, 0.20, 0.24, 0.30, 0.53 and 0.73 m, for an initial bed height, H_0, of 0.2 m. Runs have been carried out at the minimum spouting velocity, i.e., at 3.86, 3.42 and 2.54 m/s for the configuration without draft tube and those equipped with open-sided draft tube

and nonporous draft tube, respectively. The tip of the borescope is placed at the first measuring point (contactor or confiner wall, depending on the height) and is subsequently displaced step-by-step in the radial direction every centimetre. A total of four recordings have been carried out at each measuring point and all the runs have been repeated at least twice in order to obtain reliable results.

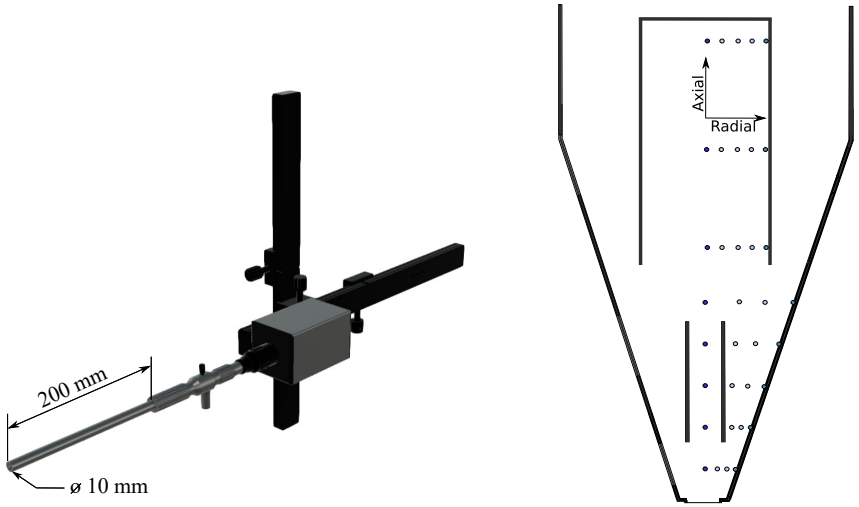

Figure 2: Description of (a) the borescope assembly with its main dimensions and (b) locations in which the vertical component was measured.

Solid velocities are obtained through the detection of the solid optical flow, Figure 3, for which the aforementioned borescope is used. Subsequently, these images are fed into a solid detection algorithm in which particle locations are identified for consecutive frames. Based on a minimization of the total solid displacement, particles are paired in the frames and the optical displacement is obtained. Considering that spouted beds mainly have vertical solid displacement in the annulus, spout and most of the fountain region, this optical displacement has been related to the solid velocity based on pixel distances and frame recording rates. The most challenging aspect of this algorithm lies in the identification of the solids, given that it depends on their shape and packing conditions. Thus, different codes for image treatment have been used depending on the spouted

bed region. On the one hand, in the dense zone (annulus), particles descend in a moving bed and individual particle rotations are negligible. Thus, Farneback pyramidal algorithm [51] from OpenCV has been found to be especially suitable to average edge movements. On the other hand, in the dilute regions (spout and fountain), particles have been tracked using a dynamic histogram equalization and a canny edge detection, which identifies closed regions as individual particles. Finally, the code locates and stores the centroids and surface projections of each region. This routine is repeated at each frame and the velocity of each particle is calculated. Thus, the average vertical particle velocity is calculated for each recording. The algorithms have been validated by comparing their output values with specific calibration measurements, which allowed confirming an error below 10% of the nominal value [39].

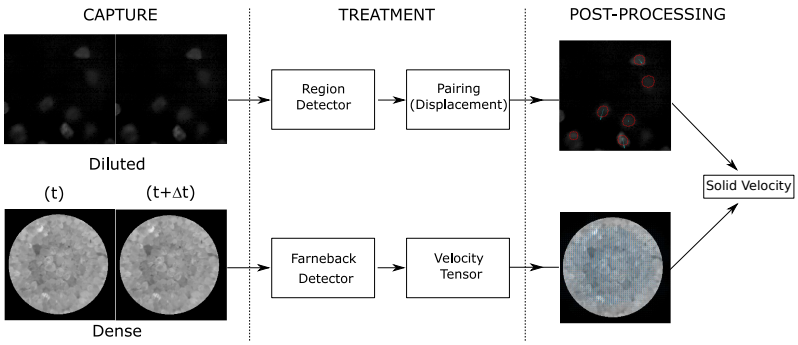

Figure 3: Graphical representation of the solid velocity capture method.

Furthermore, pressure fluctuation signals have been sampled at $1\,kHz$ using a differential pressure sensor (type $PD23$, $Keller$) with the probes inserted at the contactor inlet and outlet. Based on the data obtained by both the high speed camera and the pressure sensor, the analysis of fluctuation signals and spectral analysis (power spectral analysis) have been carried out to compare the information of both techniques and describe the dynamic behaviour of the different configurations.

3. Results

Experimental runs have been carried out using a high speed camera fitted to a borescopic system in a fountain confined conical spouted bed. Fine particles inside the contactor have been recorded at different axial and radial positions, which has allowed determining their flow pattern in the different spouted bed zones, i.e., spout, fountain, and annular zones. Using a custom particle tracking algorithm [39], mean vertical particle velocities have been determine at each location, and therefore the radial and axial particle velocity profiles in the bed. Based on the radial velocity profiles at all heights, spout-annulus and fountain core-periphery interfaces have been defined for each configuration. This information allowed delineating the spout shape and calculating the average spout diameter for each configuration.

3.1. Particle flow dynamics

The operation of fine particles in a fountain confined conical spouted bed is characterized by a pulsating pattern due mainly to temporal changes in the incorporation of particles from the annulus into the spout [15]. Accordingly, the particle movement in both the annulus and the spout is not uniform, but follows a pulse trend. Figures 4a-4c show as an example the evolution of the vertical particle velocity with time in the annular zone for different configurations at $0.20\,m$ height and $r/R = 1$ radial position (contactor wall).

As shown in Figures 4a-4c, particle velocity has an oscillatory evolution with time on the wall of the contactor at the upper surface of the annular zone, especially in the configurations without draft tube and with the open-sided draft tube (Figures 4a and 4b). Thus, particles accelerate until a maximum downward velocity is reached, and they then decelerate to reach again zero velocity. At this moment, they rest for a very short time and begin a similar trend, but upwards, i.e., they accelerate and decelerate upwards and, finally, the cycle ends with a short solid stop. Albeit this oscillatory nature of the solid movement in the annular zone, the net solid movement is downwards, thus enabling solid circulation in the contactor.

Liu et al. [5] observed a similar solid motion trend in a two-dimensional spouted bed using $d_p = 2\,mm$ glass beads. They reported that particles in the annulus showed a periodical downward movement (acceleration, deceleration and stagnation) due to incoherent spouting [52]. This regime produces periodical changes in the spout shape, as well as periodical particle movement in the annulus. In the configurations analyzed in this paper, the spout seems to undergo periodical contraction-expansion, which is responsible for the trend observed in the annulus.

Similarly, bed pressure drop measurements have been registered for each configuration. As shown in Figures 4a-4c, an analogous oscillatory dynamics is observed for all the configurations. The oscillations in pressure drop in the configurations without draft tube (Figure 4a) and with open-sided draft tube (Figure 4b) are more pronounced than in the one with nonporous draft tube (Figure 4c). This fact is explained by both the low percolation of air into the annulus and the dilute spout due to limited solid transfer from the annulus into this zone.

Based on the power spectral density (PSD), dominant frequencies have been determined in both particle velocity and pressure drop time-series signals, Figures 4d-4f. A similar main signal harmonic is observed for pressure drop and particle velocity signals, and this applies to all configurations (Figures 4d-4f), which means velocity and pressure fields are related. The main harmonic in the configuration without draft tube is detected at $6.96\,Hz$, whereas it shifts to $7.12\ Hz$ and $7.24\ Hz$ in the configurations with open-sided and nonporous draft tubes, respectively. The fact that the nonporous configuration has the highest oscillation frequency is related to its higher spouting stability, whereas similar oscillation frequencies for the three configurations evidence a similar spouting dynamics.

Figure 5 shows the evolution of particle velocity with time at the same bed height ($0.20\,m$), but at an intermediate position in the annulus ($r/R = 0.64$, i.e., $40\,mm$ from the contactor wall), for the three configurations analyzed. Similarly as on the wall, particle velocity in the inner of the annulus is fluctuating in

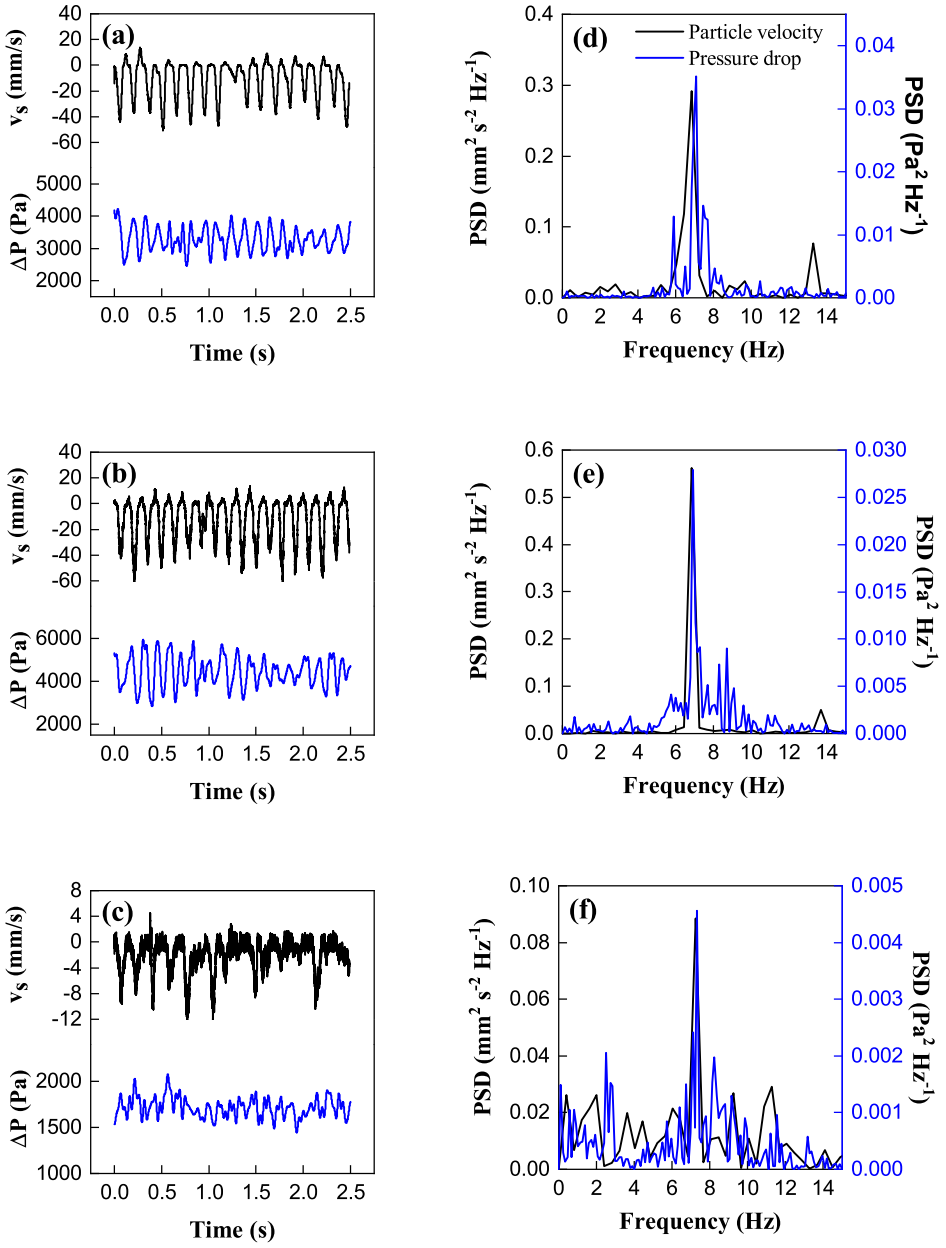

Figure 4: Vertical particle velocity and pressure drop fluctuation vs. time in the annulus for the configurations (a) without tube, (b) with open-sided tube, and (c) with nonporous tube; and signal intensity vs. frequency for the configurations (d) without tube, (e) with open-sided tube, and (f) with nonporous tube, at $0.20\,m$ height and $r/R = 1$ radial position.

the three configurations. Nevertheless, the amplitudes of the signals are much greater than those in Figures 4a-4c, which means particles move faster than on the wall. This applies especially to the configurations without draft tube and with open-sided draft tube, which is due the spout effect (particles incorporation into the spout). However, the oscillation frequency does not change with bed position, which means that this parameter is characteristic of the system.

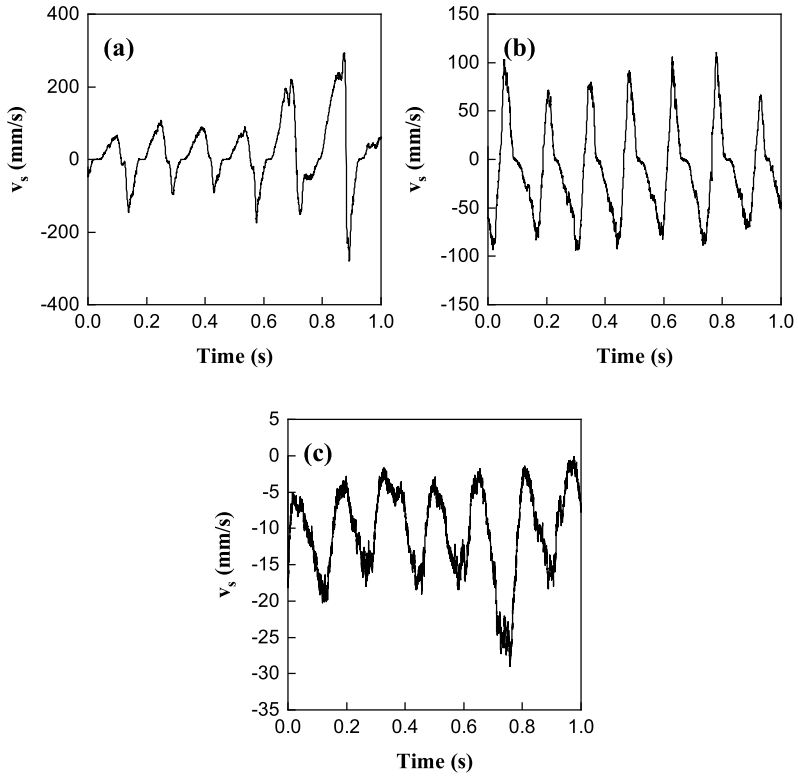

Figure 5: Vertical particle velocity vs. time for the configurations (a) without tube, (b) with open-sided tube, and (c) with nonporous tube at $0.20\,m$ height and $r/R = 0.64$ radial position.

This oscillatory solid movement is much more significant than in the case of coarse particles and greatly enhances heat and mass transfer rates in the annulus of the spouted bed. Therefore, it is a point of high relevance that should be considered in the design and application of these contactors.

Furthermore, particle velocity fluctuations also occur in the spout and foun-

tain core zones, as shown in Figure 6a. Unlike the annulus, particles in these zones show mainly upward movement, in which each cycle consists of particle acceleration to a peak velocity, deceleration to zero and a short period with almost zero velocity. This fact is explained by the bubbling-like nature of the spouting regime of this material, with particles moving as clusters and being accelerated by bursts of air that periodically expand and contract the spout. In the case of the fountain region, the amplitude of the oscillations is significantly lower due to the lower air velocity in this zone. Concerning the frequency of the oscillations, Figures 4d and 6b show that particles oscillate under the same frequency in the different zones of the spouted bed (annulus, spout, and fountain).

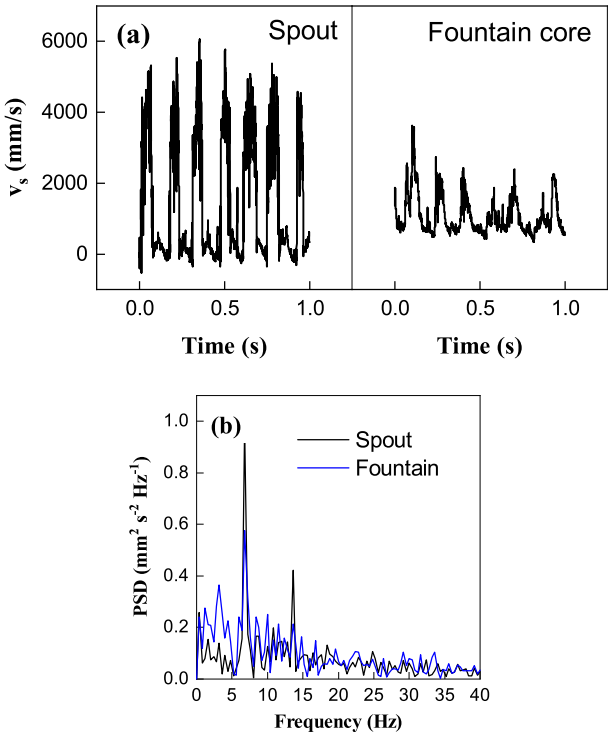

Figure 6: (a) Evolution of vertical particle velocity vs. time in the spout and fountain core and (b) their respective power spectral distribution vs. frequency, for the configuration without draft tube.

3.2. Radial and axial particle velocity profiles

Based on particle velocity fluctuation data, average solid velocities have been calculated at the different positions in the bed. Figure 7 shows an example of the radial particle velocity profiles for different configurations at the minimum spouting velocity. They correspond to a height of $0.20\,m$ in the bed and $0.30\,m$ in the fountain, both from the bottom of the bed.

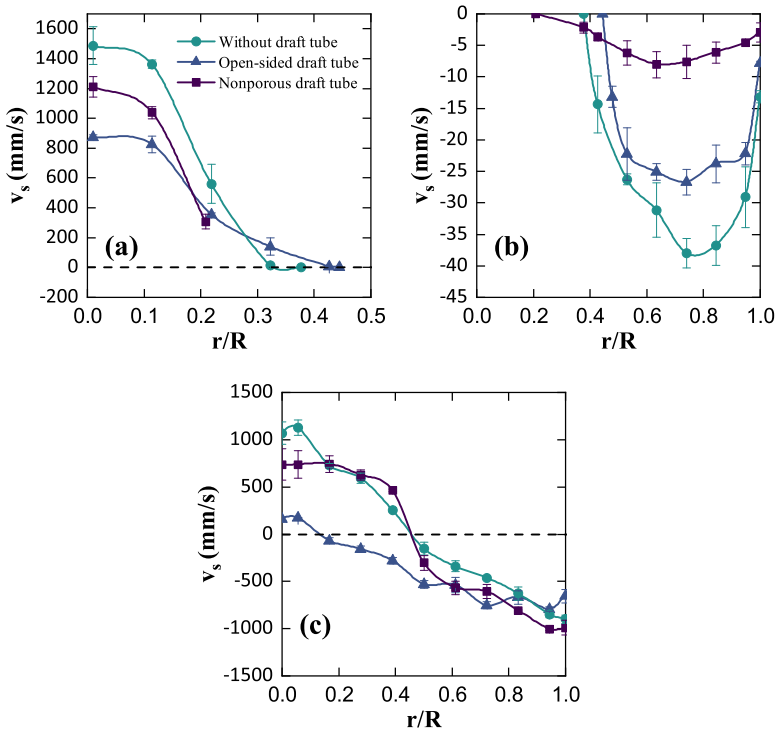

Figure 7: Radial particle velocity profile in the (a) spout ($H = 0.20\,m$), (b) annulus ($H = 0.20\,m$) and (c) fountain ($H = 0.30\,m$) for the different configurations at the minimum spouting velocity.

As shown in Figure 7, the radial profile greatly changes depending on the spouted bed region. Figure 7a shows the radial particle velocity profile in the spout region for the three configurations studied. In this zone, the particles move upwards and the velocity decreases from its maximum value at the axis to zero at the spout-annulus interface. It should be noted that this peak velocity

was slightly off centered from the axis in certain systems [53, 28]; that is, the velocity at the axis is slightly lower than that the maximum observed around the axis. Overall, there is a velocity plateau around the axis, which is evidence of spout uniformity around the axis. At radial positions further this plateau, there is a sharp decrease in velocity, and close to the spout-annulus interface the velocity and its gradient get reduced, becoming zero at the interface itself. Therefore, the shape of the radial profiles in the spout region are much closer to a Gaussian shape [53, 5, 52] than to a parabolic one [13, 54].

Solid velocities in the annulus are downward and much lower than in the spout, thereby the radial profile being significantly smoother (Figure 7b). Furthermore, given the great expansion of the spout in the open-sided draft tube configuration, the annular region gets significantly reduced. Nevertheless, it should be noted that the probe was inserted from the contactor wall towards its axis through the opened surface of the draft tube wall. Therefore, the mentioned spout expansion is a consequence of the opened section of the draft tube. The remaining two configurations have a greater annulus size, with the one for the nonporous draft tube configuration being slightly larger, as this device strictly limits the separation between annular and spout regions. This limitation hinders solid transfer from the annulus into the spout (except at the bottom section in which there is the entrainment zone), and therefore hinders spout expansion. Furthermore, given that the configurations without draft tube and with open-sided draft tube are those with the highest solid circulation rate, their maximum downward velocities in the annulus (inverse peaks in Figure 7b) are much more pronounced than for the nonporous draft tube configuration, and are located at a higher radial position (closer to the contactor wall, which is a consequence of the higher expansion of the spout. Regardless of the configuration, the maximum downward velocity is located at intermediate position in the annulus (approximately half way between the contactor wall and the spout-annulus interface [55]). Nevertheless, several authors found the maximum downward velocity close to the annulus-spout interface [56, 53, 29, 5, 57, 58, 52, 54, 59]. Details on this interface (spout size and shape) will be discussed in the next sec-

tion. In all cases, the low velocity at the wall is a consequence of the solid-wall friction.

Finally, Figure 7c shows the radial particle velocity profiles in the fountain region for the different configurations at the height of $0.30\,m$ from the bottom. It should be noted that the radial profile at this height is delimited by the wall of the fountain confiner. The particles in the fountain core travel upward, whereas those in the fountain periphery do it downward. Furthermore, the solids coming from the spout decelerate due to the expansion of the dilute zone in the fountain and the lower gas velocity. The magnitude of the upward and downward velocities is of the same order. As observed in Figure 7c, the radial profile in the fountain decreases according to a quasi-linear fashion, with the maximum upward velocity being at the axis and the maximum downward velocity at the confiner wall. An interesting fact concerning the configuration with the open-sided draft tube is that almost the entire velocity profile corresponds to downward velocities, i.e., the volume of the fountain periphery is approximately 6 times greater than the volume of the core region. This trend has been observed in all configurations with the open-sided draft tube. This explains the much lower fountain heights obtained with coarse particles when this draft tube was used without fountain confiner [60].

Figure 8 shows the profile of particle velocity along the contactor axis. As observed, particles accelerate from the bottom to approximately the top of the spout, i.e., the solids attain their maximum velocity close to the height corresponding to the static bed ($H_0 = 0.20\,m$) [61], especially in the configurations without draft tube and with open-sided draft tube. Nevertheless, when the non-porous draft tube is used, particles start to decelerate in the upper zone of the spout due to the lower minimum spouting velocity required in this configuration. That is, the air does not have enough momentum to keep accelerating the solids. Furthermore, once the particles reach the height of the static bed (H_0), a sharp velocity decrease occurs because they leave the spout and are dispersed in the fountain region.

Although a highly non-uniform axial profile has been observed in this study,

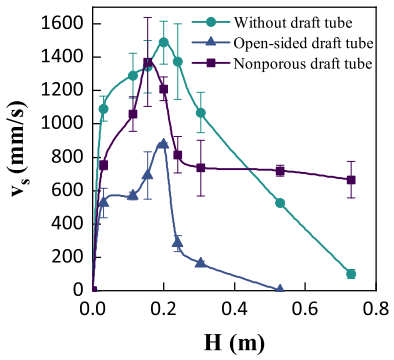

Figure 8: Particle velocity profile along the axis in the three configurations at the minimum spouting velocity.

different trends have been reported in the literature. Thus, more uniform profiles have been obtained based on the experimentation in two-dimensional spouted beds [5, 52, 54, 62]. These authors observed that particles are rapidly accelerated near the inlet zone, and they then follow an almost flat or slightly increasing trend, with the maximum solid velocity being attained at end of the spout. Other authors found the maximum particle velocity close to the inlet orifice, with particles decelerating from this point to the top of the fountain [28, 63]. Therefore, the location of this peak velocity is a consequence of several system properties, as are: static bed height, particle properties (particle diameter and solid density) and air flow rate [53].

As mentioned in the radial profiles in the dilute zones (Figures 7a and 7c), the highest particle velocities are attained when the configuration without tube is used, whereas the lowest are attained with the open-sided draft tube, which is explained by the the formation of a low and dense [60] fountain in the latter configuration. Finally, the configuration with the nonporous tube leads to velocity values in the bed (up to the bed surface) that are half way between the other configurations. Furthermore, this configuration is known because most of the air flow rate in the feed is driven through the draft tube, which leads to high particle velocities in the upper zone of the fountain, i.e., higher than those in the configuration without draft tube.

3.3. Spout and fountain geometry

Based on the radial measurements conducted at different heights, the spout-annulus and fountain core-periphery interfaces have been delineated. In order to find the transition surface, the radial positions at which particle velocity is zero have been determined in both the bed (spout-annulus) and the fountain (core-periphery) [3, 64, 59]. Figure 9 shows the spout-annulus and the fountain core-periphery interfaces for the configurations studied at the minimum spouting velocity.

As shown in Figure 9, both spout and fountain core shapes are different depending on the configuration. In the case of the configuration without draft tube (Figure 9a), a great expansion is observed at the bottom of the spout and at the upper zone in the fountain. In the remaining positions in the spout and fountain, there is a slight and steady expansion. In general, the shape of the spout found in the literature has a neck at an intermediate bed level [28, 13, 55, 47, 65, 30, 48], but the trend found in this study is similar to that reported by Mukhlenov and Gorshtein [3, 66].

Moreover, Figure 9 shows the radial particle velocity profile at different heights. In the case of the configuration without draft tube (Figure 9a), at the bottom of the spout ($H = 0.03\,m$) there is a sharp increase in velocity from the interface to radial positions around the axis of the spout. In fact, the maximum velocity is located around the axis. This fact shows that particles accessing the spout at this height are being accelerated, which leads to this highly non-uniform solid velocity profile. Nevertheless, as particles move up along the spout, the velocity profile flattens, especially above the bed surface [28, 29, 55, 63]. Finally, the velocity of the particles descending through the fountain periphery is higher as they approach the bed surface [3, 28, 58].

The shapes of the spout and fountain core are significantly different when open-sided tubes are used. As shown in Figure 9b, in the lower half of the bed, the spout expands steadily as particles are moving upward, but there is a sudden sharp expansion in the upper half of the bed, until the bed surface. It should be noted that this expansion corresponds to the open fraction of the tube wall (the

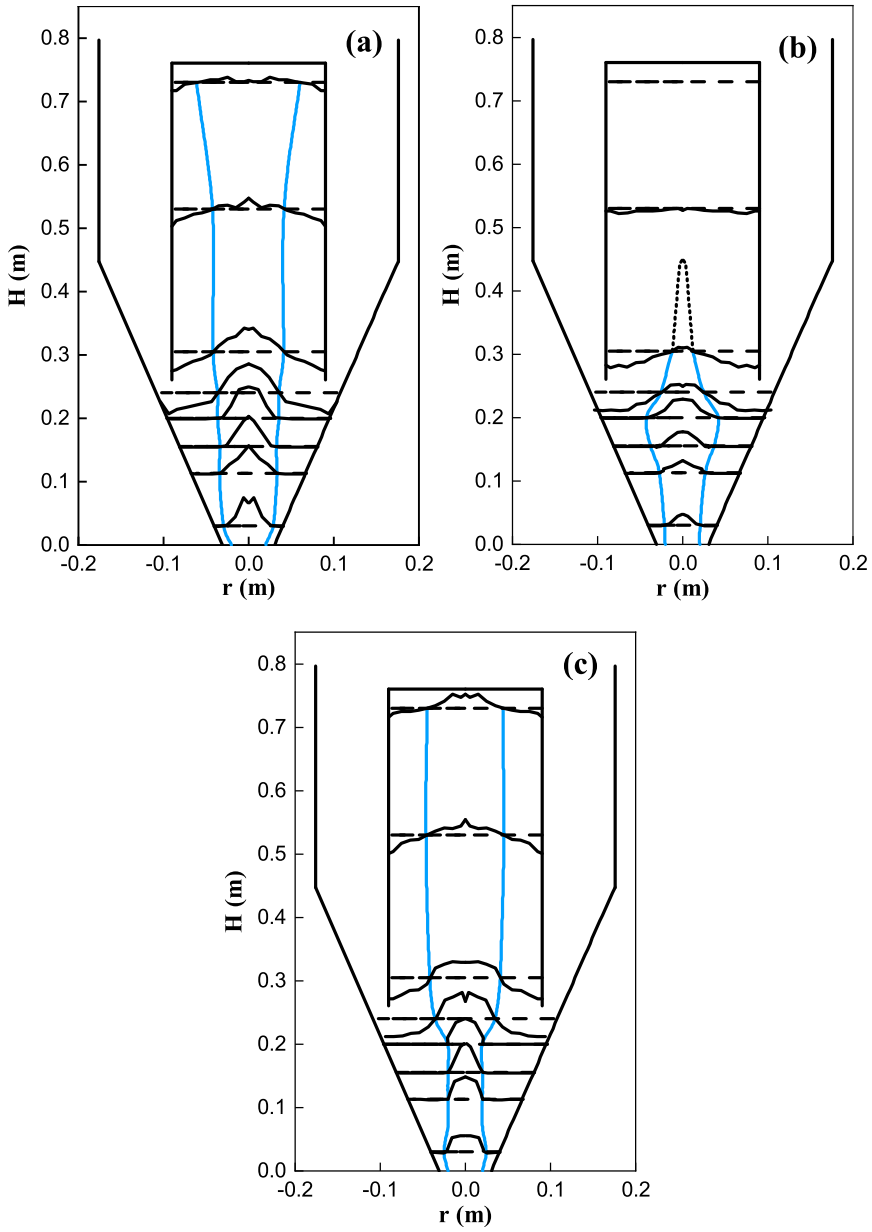

Figure 9: Spout-annulus and fountain core-periphery interfaces, and the radial particle velocity profiles at different heights in the spout and fountain for the configurations (a) without tube, (b) with open-sided tube and (c) with nonporous tube operated at the minimum spouting velocity.

remaining fraction cannot expand due to the wall of the tube). From the bed level to the top of the fountain, the core gets narrower as particles ascend along the fountain. Due to the stability provided by this tube, a great number of particles circulate through the spout, which results in a low and dense fountain.

Finally, the spout and fountain core geometries have been analysed in the configuration with a nonporous draft tube. As shown in Figure 9c, the wall of the tube defines the spout zone, and so there is no expansion along the bed. Nevertheless, a slight expansion is observed at the bottom of the spout ($H = 0.03\,m$), but it contracts to the size of the tube as particles move upward. Once the particles enter in the fountain zone, a sudden great expansion is observed until the core attains a considerable size, which keeps approximately constant up to the top of the confiner. The radial velocity profile at the bottom of the spout is almost flat, which suggests a uniform particle velocity. As particles rise through the spout and undergo collisions and friction with the draft tube wall, this uniformity changes to a pointed distribution with a maximum value located at the axis of the spout. In the fountain core, particle velocity reduces as the solids approach the top of the confiner, and those that are descending along the fountain periphery are accelerated due to gravity and air leaving the confiner.

The cross-sectional spout shape is symmetric to the axis for the configurations without draft tube and with nonporous draft tube, i.e., the radial particle velocity profile does not change around the central axis. However, open-sided draft tubes have a fraction of the wall opened, which allow solid and gas cross-flow between annulus and spout regions. In the same way, the non-opened fraction of the tube partially supports the bed, promoting stable operation with different types of solids. Furthermore, particles descending in the annulus are somewhat influenced by the air that trickles through the opened faces of the open-sided draft tube. In order to study the effect of the openings on the shape of the spout, the cross-sectional shape has been determined at various bed heights, Figure 10.

As shown in Figure 10, a three-pointed star spout shape is observed when an open-sided draft tube is used. As the air moves up along the spout, this zone

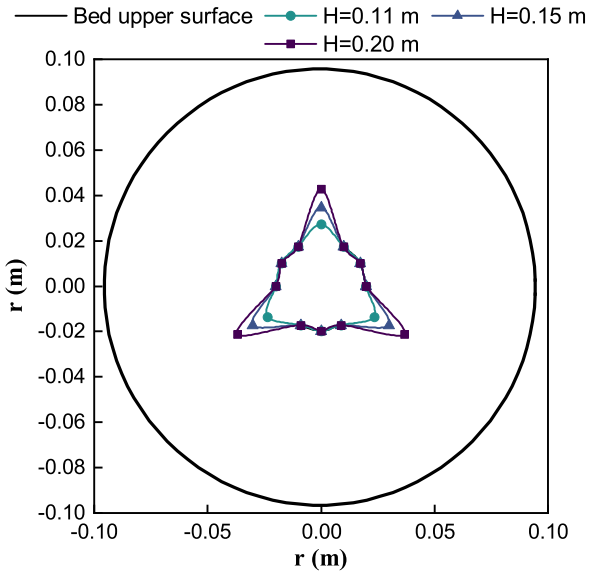

Figure 10: Cross-sectional spout shape in the configuration with the open-sided draft tube operated at the minimum spouting velocity.

expands through the opened faces of the tube. The shape of the spout shown in Figure 9b is obtained measuring across the opened face of the tube. However, the particles move downward on the outside of the non-opened fraction of the tube. Therefore, at the minimum spouting velocity, the shape of the spout along the non-opened fraction is delimited by the tube wall.

Therefore, depending on the configuration used, the spout shows a different shape and expansion zones. The average area of the spout has been measured at different heights to calculate the average spout diameter for the configurations studied. It should be noted that, as the main part of the spout in the configuration with the nonporous draft tube is delimited by the tube wall, the average spout diameter is very similar to the diameter of the internal device. Accordingly, the average spout diameter has been calculated for the rest of the configurations at the minimum spouting velocity. Table 2 shows the error obtained for the literature correlations listed in Table 1.

As shown in Table 2, the average spout diameter obtained for the configuration without draft tube is 1.36 times greater than what obtained for the

configuration with the open-sided draft tube. In the latter case, the tube partially hinders air diversion into the annulus and solid cross-flow from the annulus into the spout, which have an influence on spout expansion. In the case of the configuration without draft tube, the absence of internal device to support the bed and drive the particles along the spout involves the highest air velocity requirement for minimum spouting, which then results in a greater bed expansion.

Most of the correlations listed in Table 1 under-predict the average spout diameter for the configurations studied in this work. These correlations have been developed mainly with data from experiments carried out with coarse granular materials [36, 46, 43, 40, 44, 41], but also with different configurations (cylindrical [47, 48] and semicircular [43, 40, 44]) and operating conditions [35] to those used here. In this work, fine particles have been used, which lead to a great expansion of the spout. This suggests that the poor prediction of the correlations in the literature are mainly attributed to the low average diameter of the sand particles used, which is well below the range used to propose the aforementioned correlations. In fact, operation with these particles is not feasible in a standard spouted bed, but a fountain confiner is required, which was not the case in any of the correlations proposed.

The correlations proposed by San José et al. [48] and Volpicelli et al. [42] are the ones of best fit to the experimental results for the configurations without draft tube and with open-sided draft tube, respectively. In the case of San José et al., they used a similar contactor geometry (conical spouted bed) to that used in this work and, furthermore, Equation 13 is the only one that takes into account the upper diameter of the bed (D_b) instead of the column diameter (D_C). Finally, the correlation by Volpicelli et al.[42] provided the best fit for the configuration without draft tube and, although they operated with a rectangular faced two-dimensional contactor, they also reported gas bubbling and solid clustering that moved in a ripple like fashion from the bottom of the bed to the fountain region, thus creating several necks and expansion zones in the spout, resulting in an increased average spout diameter.

Table 2: Comparison of the experimental average spout diameters with those predicted by the literature correlations.

Correlation	Configuration	$\overline{D_s}$ (m)	$\overline{D_{s,exp}}$ (m)	Error (%)
Malek et al. (1963)	Without	0.003	0.061	95.08
	Open-sided	0.003	0.045	93.33
Mikhailik (1966)	Without	0.017	0.061	72.13
	Open-sided	0.016	0.045	64.44
Volpicelli et al. (1967)	Without	0.055	0.061	9.83
	Open-sided	0.052	0.045	15.55
Lefroy and Davidson (1669)	Without	0.032	0.061	47.54
	Open-sided	0.032	0.045	28.88
Abdelrazek (regular particles) (1969)	Without	0.159	0.061	160.65
	Open-sided	0.152	0.045	237.77
Abdelrazek (irregular particles) (1969)	Without	0.207	0.061	239.34
	Open-sided	0.195	0.045	333.33
McNab (1972)	Without	0.023	0.061	62.29
	Open-sided	0.021	0.045	53.33
Bridgwater and Mathur (1972)	Without	0.013	0.061	78.68
	Open-sided	0.012	0.045	73.33
Green and Bridgwater (1983)	Without	0.025	0.061	59.01
	Open-sided	0.023	0.045	48.88
Wu et al. (1987)	Without	0.023	0.061	62.29
	Open-sided	0.021	0.045	53.33
San José et al. (2001)	Without	0.017	0.061	72.13
	Open-sided	0.017	0.045	62.22
San José et al. (2005, shallow)	Without	0.015	0.061	75.41
	Open-sided	0.014	0.045	68.88
San José et al. (2005, conical)	Without	0.050	0.061	18.03
	Open-sided	0.049	0.045	8.88

4. Conclusion

The fountain confiner allows operating with fine particles, but the gas-solid contact is characterized by a pulsating regime. In this situation, an oscillatory trend is observed in the spout and fountain dynamics. Moreover, particles that are going down through the annulus also show an oscillatory movement, i.e., they are moving downwards and upwards. Due to this oscillatory movement, gas-solid contact is greatly improved in the annulus, which is a fact to be considered when designing applications based on conical spouted beds.

The shape of the radial particle velocity profiles differs depending on the spouted bed region. In the annulus, the radial profile shows a parabolic trend and the maximum downward velocity is located at intermediate positions (approximately half way between the contactor wall and the spout-annulus interface) in all the configurations studied. In the spout, the velocity profiles follow a Gaussian-like curve, with the maximum upward velocity being located at the axis or close to it, which is also the case in the fountain core. Furthermore, particles accelerate in the spout and they then decelerate along the fountain. Among the three configurations studied, the highest particle velocities are observed in the configuration without tube.

The air is driven along the spout in different ways depending on the configuration used. In the configurations without draft tube, a great expansion occurs at the spout bottom, which is then further expanded above the bed surface. The spout cannot expand along the bed in the configuration with the nonporous draft tube, as the tube wall hinders gas and solid interchange, but expansion beyond the limits of the tube wall occurs in the entrainment height and fountain region. Finally, a great expansion is observed in the upper half of the bed when a configuration with open-sided draft tube is used, but, once the spout ends, the fountain core narrows and a low and dense fountain is obtained. Moreover, the draft tube openings enable air trickling to the annulus, which leads to a three-pointed star shaped spout. Most of the literature correlations for estimating the average spout diameter under-predict the results obtained in

this work and those by San José et al. [48] and Volpicelli et al. [42] provide the best fit in the configurations without draft tube and with open-sided draft tube, respectively, with their relative errors being 9.83% and 8.88% respectively.

Acknowledgements

This work has received funding from Spain's Ministry of Economy and Competitiveness (CTQ2016-75535-R (AEI/FEDER, UE)) and Science and Innovation (PID2019-107357RB-I00 (AEI/FEDER, UE)), and the European Commission (HORIZON H2020-MSCA RISE-2018. Contract No.: 823745). M. Tellabide thanks Spain's Ministry of Education, Culture and Sport for his Ph.D. grant (FPU14/05814). I. Estiati thanks the University of the Basque Country for her postgraduate grant (ESPDOC18/14). A. Atxutegi is grateful for his Ph.D. grant from the University of the Basque Country UPV/EHU (PFI15-2017).

References

[1] K. B. Mathur, P. E. Gishler, A study of the application of the spouted bed technique to wheat drying, Journal of Applied Chemistry 5 (11) (1955) 624–636. doi:10.1002/jctb.5010051106.

[2] J. F. Saldarriaga, A. Atxutegi, R. Aguado, H. Altzibar, J. Bilbao, M. Olazar, Influence of contactor geometry and draft tube configuration on the cycle time distribution in sawdust conical spouted beds, Chemical Engineering Research and Design 102 (2015) 80–89. doi:10.1016/j.cherd.2015.05.042.

[3] X. Chen, B. Ren, Y. Chen, W. Zhong, D. Chen, Y. Lu, B. Jin, Distribution of particle velocity in a conical cylindrical spouted bed, Canadian Journal of Chemical Engineering 91 (11) (2013) 1762–1767. doi:10.1002/cjce.21850.

[4] R. C. Sousa, M. C. Ferreira, H. Altzibar, F. B. Freire, J. T. Freire, Drying of pasty and granular materials in mechanically and conventional spouted beds, Particuology 42 (2019) 176–183. doi:10.1016/j.partic.2018.01.006.

[5] G. Q. Liu, S. Q. Li, X. L. Zhao, Q. Yao, Experimental studies of particle flow dynamics in a two-dimensional spouted bed, Chemical Engineering Science 63 (4) (2008) 1131–1141. doi:10.1016/j.ces.2007.11.013.

[6] O. M. Dogan, L. A. P. Freitas, C. J. Lim, J. R. Grace, B. Luo, Hudrodynamics and Stability of Slot-Rectangular Spouted Beds. Part I: Thin Bed (September 2014) (2000) 37–41. doi:10.1080/00986440008912822.

[7] M. J. San José, M. Olazar, A. T. Aguayo, J. M. Arandes, J. Bilbao, Expansion of spouted beds in conical contactors, The Chemical Engineering Journal 51 (1) (1993) 45–52. doi:10.1016/0300-9467(93)80007-B.

[8] R. C. Brito, M. B. Zacharias, V. A. Forti, J. T. Freire, Physical and physiological quality of intermittent soybean seeds drying in the spouted bed, Drying Technology (2020). doi:10.1080/07373937.2020.1725544.

[9] J. Alvarez, B. Hooshdaran, M. Cortazar, M. Amutio, G. Lopez, F. B. Freire, M. Haghshenasfard, S. H. Hosseini, M. Olazar, Valorization of citrus wastes by fast pyrolysis in a conical spouted bed reactor, Fuel 224 (July 2017) (2018) 111–120. doi:10.1016/j.fuel.2018.03.028.

[10] M. Pozitano, S. C. Dos Santos Rocha, Fluid dynamic and polymeric coating of forest seeds of senna macranthera (collad.) irwin et barn in conical spouted bed, Chemical Engineering Transactions 24 (2011) 667–672. doi:10.3303/CET1124112.

[11] M. J. San José, S. Alvarez, R. López, Catalytic combustion of vineyard pruning waste in a conical spouted bed combustor, Catalysis Today 305 (2018) 13–18. doi:10.1016/j.cattod.2017.11.020.

[12] G. Lopez, J. Alvarez, M. Amutio, A. Arregi, J. Bilbao, M. Olazar, Assessment of steam gasification kinetics of the char from lignocellulosic biomass in a conical spouted bed reactor, Energy 107 (2016) 493–501. doi:10.1016/j.energy.2016.04.040.

[13] K. B. Mathur, N. Epstein, N. Mathur, K. B., Epstein, Spouted Beds, academic Edition, Academic Press Incorporated,U.S., New York, 1974.

[14] M. Olazar, M. J. San Jose, A. T. Aguayo, J. M. Arandes, J. Bilbao, Stable operation conditions for gas-solid contact regimes in conical spouted beds, Industrial & Engineering Chemistry Research 31 (7) (1992) 1784–1792. doi:10.1021/ie00007a025.

[15] M. Tellabide, I. Estiati, A. Pablos, H. Altzibar, R. Aguado, M. Olazar, New operation regimes in fountain confined conical spouted beds, Chemical Engineering Science 211 (2020). doi:10.1016/j.ces.2019.115255.

[16] T. Al-Juwaya, N. Ali, M. Al-Dahhan, Investigation of cross-sectional gas-solid distributions in spouted beds using advanced non-invasive gamma-ray computed tomography (CT), Experimental Thermal and Fluid Science 86 (2017) 37–53. doi:10.1016/j.expthermflusci.2017.03.029.

[17] T. Al-Juwaya, N. Ali, M. Al-Dahhan, Investigation of hydrodynamics of binary solids mixture spouted beds using radioactive particle tracking (RPT) technique, Chemical Engineering Research and Design 148 (2019) 21–44. doi:10.1016/j.cherd.2019.05.051.

[18] N. Ali, T. Al-Juwaya, M. Al-Dahhan, Demonstrating the non-similarity in local holdups of spouted beds obtained by CT with scale-up methodology based on dimensionless groups, Journal of Mathematical Psychology 59 (2016) 129–141. doi:10.1016/j.cherd.2016.08.010.

[19] L. Godfroy, F. Larachi, G. Kennedy, B. Grandjean, J. Chaouki, On-line flow visualization in multiphase reactors using neural networks, Applied Radi-

ation and Isotopes 48 (2) (1997) 225–235. doi:10.1016/S0969-8043(96)00183-2.

[20] T. Kawaguchi, MRI measurement of granular flows and fluid-particle flows, Advanced Powder Technology 21 (3) (2010) 235–241. doi:10.1016/j.apt.2010.03.014.

[21] H. C. Park, H. S. Choi, Visualization of flow structures inside a conical spouted bed by electrical capacitance volume tomography, Particuology 42 (2019) 15–25. doi:10.1016/j.partic.2018.01.002.

[22] D. Roy, F. F. Larachi, R. Legros, J. Chaouki, Study of solid behavior in spouted beds using 3-D particle tracking, Canadian Journal of Chemical Engineering 72 (6) (1994) 945–952. doi:10.1002/cjce.5450720602.

[23] L. Spreutels, B. Haut, R. Legros, F. Bertrand, J. Chaouki, Experimental investigation of solid particles flow in a conical spouted bed using radioactive particle tracking, AIChE Journal 62 (1) (2015) 26–37. doi:10.1002/aic.15014.

[24] E. E. Patterson, J. Halow, S. Daw, Innovative Method Using Magnetic Particle Tracking to Measure Solids Circulation in a Spouted Fluidized Bed, Industrial & Engineering Chemistry Research 49 (11) (2010) 5037–5043. doi:10.1021/ie9008698.

[25] G. Mohs, O. Gryczka, S. Heinrich, L. Mörl, Magnetic monitoring of a single particle in a prismatic spouted bed, Chemical Engineering Science 64 (23) (2009) 4811–4825. doi:10.1016/j.ces.2009.08.025.

[26] S. Aradhya, H. Taofeeq, M. Al-Dahhan, A new mechanistic scale-up methodology for gas-solid spouted beds, Chemical Engineering and Processing: Process Intensification 110 (2016) 146–159. doi:10.1016/j.cep.2016.10.005.

[27] M. A. Barrozo, C. R. Duarte, N. Epstein, J. R. Grace, C. J. Lim, Experimental and computational fluid dynamics study of dense-phase, transition

region, and dilute-phase spouting, Industrial and Engineering Chemistry Research 49 (11) (2010) 5102–5109. doi:10.1021/ie9004892.

[28] Y. L. He, S. Z. Qin, C. J. Lim, J. R. Grace, Particle velocity profiles and solid flow patterns in spouted beds, The Canadian Journal of Chemical Engineering 72 (4) (1994) 561–568. doi:10.1002/cjce.5450720402.

[29] G. Kulah, S. Sari, M. Koksal, Particle Velocity, Solids Hold-Up, and Solids Flux Distributions in Conical Spouted Beds Operating with Heavy Particles, Industrial and Engineering Chemistry Research 55 (11) (2016) 3131–3138. doi:10.1021/acs.iecr.5b04496.

[30] M. J. San José, S. Alvarez, A. O. De Salazar, M. Olazar, J. Bilbao, Spout geometry in shallow spouted beds with solids of different density and different sphericity, Industrial and Engineering Chemistry Research 44 (22) (2005) 8393–8400. doi:10.1021/ie050447m.

[31] J. Yang, R. W. Breault, J. M. Weber, S. L. Rowan, Determination of flow patterns by a novel image analysis technique in a rectangular spouted bed, Powder Technology 334 (2018) 151–162. doi:10.1016/j.powtec.2018.04.067.

[32] J. Yang, R. W. Breault, S. L. Rowan, Experimental investigation of fountain height in a shallow rectangular spouted bed using digital image analysis, Chemical Engineering Journal 380 (April 2019) (2020) 122467. doi:10.1016/j.cej.2019.122467.

[33] F. Wu, L. Shang, Z. Yu, X. Ma, W. Zhou, Experimental investigation on hydrodynamic behavior in a spouted bed with longitudinal vortex generators, Advanced Powder Technology 30 (July) (2019) 2178–2187.

[34] M. Kiani, M. R. Rahimi, S. H. Hosseini, G. Ahmadi, Mixing and segregation of solid particles in a conical spouted bed: Effect of particle size and density, Particuology 32 (2017) 132–140.

[35] S. W. Wu, C. J. Lim, N. Epstein, Hydrodynamics of Spouted Beds at Elevated Temperatures, Chemical Engineering Communications 62 (1-6) (1987) 251–268. doi:10.1080/00986448708912063.

[36] I. D. Abdelrazek, Analysis of Thermo-Chemical Deposition in Spouted Beds, Ph.D. thesis, University of Tennessee, Knoxville, TN, (1969).

[37] A. Pablos, R. Aguado, M. Tellabide, H. Altzibar, F. B. Freire, J. Bilbao, M. Olazar, A new fountain confinement device for fluidizing fine and ultrafine sands in conical spouted beds, Powder Technology 328 (2018) 38–46. doi:10.1016/j.powtec.2017.12.090.

[38] A. Pablos, R. Aguado, J. Vicente, M. Tellabide, J. Bilbao, M. Olazar, Elutriation, attrition and segregation in a conical spouted bed with a fountain confiner, Particuology (2019). doi:10.1016/j.partic.2019.08.006.

[39] A. Atxutegi, M. Tellabide, G. Lopez, R. Aguado, J. Bilbao, M. Olazar, Implementation of a borescopic technique in a conical spouted bed for tracking spherical and irregular particles, Chemical Engineering Journal 374 (May) (2019) 39–48. doi:10.1016/j.cej.2019.05.143.

[40] M. A. Malek, L. A. Madonna, B. C. Lu, Estimation of spout diameter in a spouted bed, Industrial and Engineering Chemistry Process Design and Development 2 (1) (1963) 30–34. doi:10.1021/i260005a006.

[41] V. Mikhailik, The Pattern of Change of Spout Diameter in Spouting Bed, Collected Works on Research on Heat and Mass in Technological Processes (1966) 37.

[42] G. Volpicelli, G. Raso, L. Massimilla, Gas and Solid Flow in Bidimensional Spouted Beds, Proceedings of the International Symposium on Fluidization (1967) 123.

[43] G. Lefroy, J. F. Davidson, The Mechanics of Spouted Beds, Trans. 1nst. Chem. Eng. 47 (1969) 120.

[44] G. S. McNab, Predictions of spout diameter, Br. Chem. Eng. Proc. Tech. 17 (1972) 532.

[45] J. Bridgwater, K. B. Mathur, Prediction of Spout Diameter in a Spouted Bed: A Theoretical Model, Powder Technology 6 (1972) 183.

[46] M. Green, J. Bridgwater, An Experimental Study of Spouting in Large Sector Beds, Canadian Journal of Chemical Engineering1 61 (1983) 281.

[47] M. J. San José, M. Olazar, M. A. Izquierdo, S. Alvarez, J. Bilbao, M. J. San Jose, M. A. Izquierdo, S. Alvarez, J. Bilbao, M. Olazar, M. A. Izquierdo, S. Alvarez, J. Bilbao, Spout geometry in shallow spouted beds, Industrial & Engineering Chemistry Research 40 (1) (2001) 420–426. doi:Doi10.1021/Ie000340t.

[48] M. Olazar, S. Alvarez, A. Morales, M. J. San José, M. Olazar, S. Alvarez, A. Morales, J. Bilbao, Spout and Fountain Geometry in Conical Spouted Beds Consisting, Industrial and Engineering Chemistry Research 44 (1) (2005) 193–200. doi:10.1021/ie040137o.

[49] I. Estiati, M. Tellabide, J. F. Saldarriaga, H. Altzibar, M. Olazar, Fine particle entrainment in fountain confined conical spouted beds, Powder Technology 344 (2019) 278–285. doi:10.1016/j.powtec.2018.12.035.

[50] I. Estiati, M. Tellabide, A. Pablos, H. Altzibar, R. Aguado, M. Olazar, Design Factors in Fountain Confined Conical Spouted Beds, Chemical Engineering and Processing - Process Intensification 155 (August) (2020) 108062. doi:10.1016/j.cep.2020.108062.

[51] G. Farnebäck, Fast and accurate motion estimation using orientation tensors and parametric motion models, Proceedings - International Conference on Pattern Recognition 15 (1) (2000) 135–139.

[52] H. Zhang, M. Liu, T. Li, Z. Huang, X. Sun, H. Bo, Y. Dong, Experimental investigation on gas-solid hydrodynamics of coarse particles in

a two-dimensional spouted bed, Powder Technology 307 (2017) 175–183. doi:10.1016/j.powtec.2016.11.024.

[53] T. Djeridane, F. Larachi, D. Roy, J. Chaovki, R. Legros, Investigation of the mean and turbulent particle velocity fields in a spouted bed using radioactive particle tracking, The Canadian Journal of Chemical Engineering 76 (2) (1998) 190–195. doi:10.1002/cjce.5450760205.

[54] X. L. Zhao, S. Q. Li, G. Q. Liu, Q. Yao, J. S. Marshall, DEM simulation of the particle dynamics in two-dimensional spouted beds, Powder Technology 184 (2) (2007) 205–213. doi:10.1016/j.powtec.2007.11.044.

[55] M. Olazar, M. J. San Jose, R. Llamosas, S. Alvarez, J. Bilbao, Study of Local Properties in Conical Spouted Beds Using an Optical Fiber Probe, Industrial Engineering Chemistry Research 34 (1995) 4033–4039.

[56] A. Benkrid, H. S. Caram, Solid flow in the annular region of a spouted bed, AIChE Journal 35 (8) (1989) 1328–1336. doi:10.1002/aic.690350811.

[57] M. J. San José, M. Olazar, S. Alvarez, J. Bilbao, Local bed voidage in conical spouted beds, Industrial and Engineering Chemistry Research 37 (6) (1998) 2553–2558. doi:10.1021/ie9707681.

[58] Z. Wang, H. T. Bi, C. J. Lim, Measurements of local Flow Structures of conical spouted beds by optical fibre probes, Canadian Journal of Chemical Engineering 87 (2) (2009) 264–273. doi:10.1002/cjce.20157.

[59] R. Zhu, S. Li, Q. Yao, Effect of cohesion on granular-fluid flows in spouted beds: PIV measurement and DEM simulations, AIP Conference Proceedings 1542 (2013) 979–982. doi:10.1063/1.4812097.

[60] H. Altzibar, G. Lopez, J. Bilbao, M. Olazar, Minimum Spouting Velocity of Conical Spouted Beds Equipped with Draft Tubes of Different Configuration, Ind. Eng. Chem. Res 52 (2013) 2995–3006.

[61] B. Waldie, D. Wilkinson, Measurement of particle movement in a spouted bed using a new microprocessor based technique, The Canadian Journal of Chemical Engineering 64 (6) (1986) 944–949. doi:10.1002/cjce.5450640609.

[62] X. L. Zhao, S. Q. Li, G. Q. Liu, Q. Song, Q. Yao, Flow patterns of solids in a two-dimensional spouted bed with draft plates: PIV measurement and DEM simulations, Powder Technology 183 (1) (2008) 79–87. doi:10.1016/j.powtec.2007.11.021.

[63] M. Olazar, M. J. San Jose, S. Alvarez, A. Morales, J. Bilbao, Measurement of Particle Velocities in Conical Spouted Beds Using an Optical Fiber Probe, Industrial Engineering Chemistry Research 37 (4) (1998) 4520–4527.

[64] A.-L. He, C. J. Lim, J. R. Grace, S.-Z. Qin, Spout diameters in full and half spouted beds, The Canadian Journal of Chemical Engineering 76 (4) (1998) 702–706. doi:10.1002/cjce.5450760403.

[65] M. J. San José, M. Olazar, R. Llamosas, M. A. Izquierdo, J. Bilbao, Study of dead zone and spout diameter in shallow spouted beds of cylindrical geometry, Chemical Engineering Journal 64 (3) (1996) 353–359. doi:10.1016/S0923-0467(97)80006-1.

[66] I. P. Mukhlenov, A. E. Gorstein, Investigation of a spouted bed, Kim. Prom. 41 (1965) 443–446.